Detection of Subsurface Voids in Soil Media Using Seismic Wave Methods

A. Srivastava[1], J. A. Laman[2,*], and A. Schokker[3]

[1]*ANSYS, Inc., 1007 Church Street, Suite 250, Evanston, IL 60201*

[2]*The Pennsylvania State University, Dept of Civ and Env Engrg, University Park, PA, 16802*

[3]*University of Minnesota, Duluth, MN 55812*

Abstract: This research investigated the effect of anomalies such as voids on surface wave propagation. This was achieved by studying the signal simultaneously in both the time and frequency domains with the assistance of time-frequency plots generated by continuous wavelet transformation (CWT). The study also investigated the effects of different types of wavelets on CWT and developed a protocol for processing seismic wave data for void detection. For this purpose a numerical and experimental study was conducted and the data was studied in both the time and frequency domains in conjunction with time-frequency plots. The response of the soil media is presented in the time-frequency plots. The presence of void like anomalies disrupts the time-frequency plot features and introduces new features. These features have been used for cavity detection.

Keywords: Wave propagation, void detection, continuous wavelet transformation, time-frequency plot, FDTD simulation.

1. INTRODUCTION

Detection of obstacles, voids, cavities, sub-surface rock profiles, or underground utilities is required for the planning, design, and remediation of existing sub-structures (foundations, tunnels or basements). These sub-surface features affect the soil properties in their vicinity. The design and planning process of any sub-structure is significantly dependent on these sub-surface soil properties.

Seismic wave based sub-surface exploration techniques are usually very successful in determining the soil properties surrounding the sub surface features that have significant rigidity variation [1]. These methods include multi-channel analysis of surface waves (MASW), spectral analysis of surface waves (SASW), seismic refraction survey, and seismic reflection survey. These methods are based on the travel time estimation, or spectral analysis, of the elastic waves (surface waves, compression waves and shear waves) generated in a medium due to an impact on the ground surface. Travel time based methods include the refraction and reflection method and spectral analysis methods include spectral analysis of surface waves (SASW) and multichannel analysis of surface waves (MASW).

Past research has investigated the use of seismic methods to detect subsurface voids. Cooper and Ballard (1988) [2] have shown that the presence of any cavities or anomalies near the surface tends to increase arrival time and voids can be detected using this phenomenon. However, the refraction method fails to detect soil or water-filled cavities and rigid obstacles. Belesky and Hardy (1986 [3] studied the effects of horizontal strata on arrival time and found that the phenomenon of increased arrival time due to shallow cavities cannot be applied in the case of stratified soil profiles as this procedure cannot differentiate between signals arriving from anomalies and reflections from different layers of soil media. Spectral analysis methods have been very effective and successful in determining the elastic moduli of the soil layers surrounding these ground [1]. The variations of spectral methods have also been utilized to detect sub-surface void like anomalies [3, 4, 5]. However, the effectiveness of these methods is dependant on the source location, receiver array placement and tomography of the surrounding soil [6].

The traditional spectral method approaches lack the information of spectrum variation in the time domain due to the presence of cavities and layers of soil. The spectral information of the reflected waves from any cavities or anomalies is lost when a Fourier transform is performed on seismic test data. Travel time based methods that are generally used in the case of reflection and refraction of seismic waves do not supply information about change in frequency content. Thus, analyzing the signal simultaneously in both the time and frequency domains are expected to be more efficient than analyzing it in one domain.

*Address correspondence to this author at The Pennsylvania State University, Dept of Civ and Env Engrg, University Park, PA, 16802;
Tel: (814) 863-0523; Fax: 814-863-7304; E-mail: JLAMAN@PSU.EDU

E-ISSN: 2409-5710/16

In this research, the effect of voids in soil media was examined by qualitatively comparing the signal properties acquired from controlled laboratory experiments on a soil media, both with and without voids. A data processing protocol was developed for processing seismic wave data for void detection by studying the signal simultaneously in the time and frequency domains using continuous wavelet transformation (CWT) [7]. The basic theory of CWT is also briefly discussed. In addition to the experimental study, a numerical study was also conducted using a 2D finite difference model in the Wave2000® Pro software. The present study was conducted to determine the feasibility of simulating the physical phenomenon numerically. Once established and refined, this numerical model could be used to determine the effect of different variables such as void size and heterogeneity of soil media. However, the present study is limited to the determination of concept feasibility. In the present study only a 2D model is considered because the computational requirements for a 3D wave propagation was extensive. The numerical receiver data was processed with the same protocol that was used for analyzing the experimental test data collected from the laboratory soil box with a void. The time-frequency maps constructed using the experimental data confirm the numerical results. From the experimental and numerical results it can be concluded that the time-frequency plot features generated from a CWT analysis can be used to investigate the seismic wave propagation and therefore can be used to study its properties in the presence of voids.

2. CONTINUOUS WAVELET TRANSFORMATION

Wavelet analysis is a relatively new technique that can be applied to dynamic soil response data to study signals in the time and frequency domains simultaneously. Kaiser G., (1994) [8] defined the wavelet transformation as "Wavelet transformation can be regarded as the convolution between a function known as wavelet and the original signal." A function, defined as a mother wavelet, $\Psi(t)$, is required before performing a wavelet transformation. This function must be well defined, localized in time and frequency domains, and should have a zero mean [8]. There are many types of mother wavelets developed for purposes such as time series analysis, dynamic data analysis, de-noising signals, image processing, and speech recognition [9].

A wavelet, $\psi_{a,t}(\tau)$ at time location, *t,* and to scale, *a,* and integration variable, τ, is given by the following equation [10]:

$$\psi_{a,t}(\tau) = \frac{1}{\sqrt{a}}\psi\left(\frac{t-\tau}{a}\right) \quad (1)$$

CWT $W_{\psi x}$ of any signal, *x(t),* with wavelet, $\psi(\tau)$, having range of scales, *a,* is defined as follows [10]:

$$W_{\psi}x_{a,t} = \int_{-\infty}^{+\infty} x(\tau)\psi^{*}_{a,t}(\tau)\,d\tau \quad (2)$$

where $\psi_{a,t}(\tau)$ is the complex conjugate of $\psi_{a,t}(\tau)$, $W_{\psi}x_{a,t}$ is the wavelet coefficient, and *a* is the scale of a

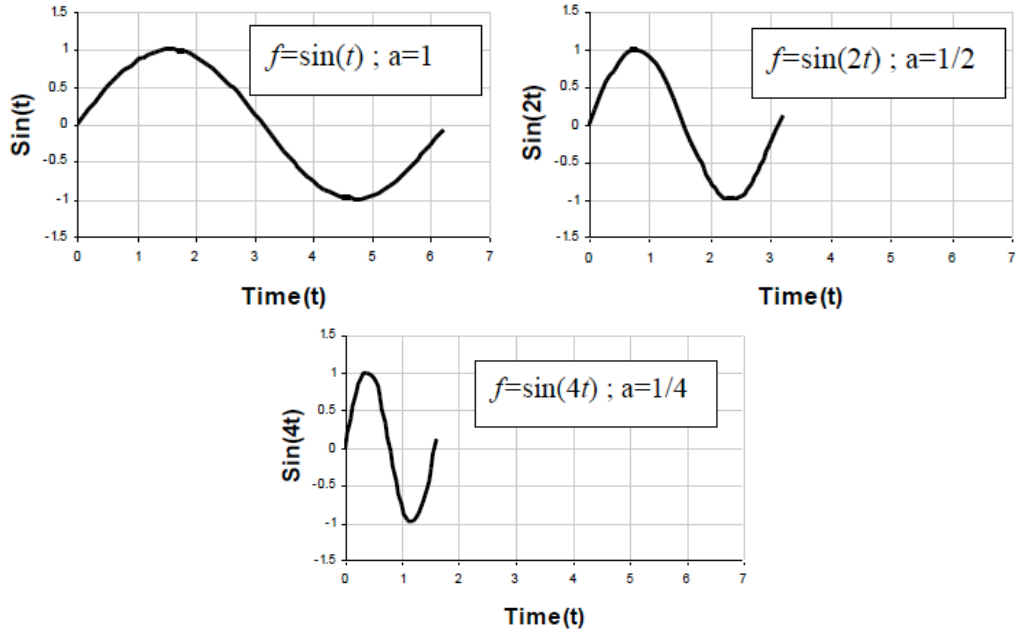

Figure 1: Sine function with different scales.

wavelet that is the inverse function of frequency. To demonstrate the functionality of scale, sine waves with different scales are plotted and presented in Figure **1**. The lower value of scale has resulted in a more compressed wave and also the radian frequency has increased. Thus, from Figure **1**, it is evident that the scale is related to the radian frequency of the sine functions.

In the case of wavelets, the scale works in the same way as in the example of sine waves presented in Figure **1**. A db2 wavelet is plotted with different scales and is presented in Figure **2**. It is clear from the plots that the small scale results in a more compressed wavelet and thus has a higher frequency content than the mother wavelet.

From Figure **2** it can also be concluded that in the wavelet analysis, the scales can be related to the frequency of the wavelet and thus can be related to the frequency of the signal. To compute the frequency relationship to the scale, the center frequency, F_c, of the mother wavelet is computed. The center frequency is determined from the power spectral density (PSD) plot of the mother wavelet. The frequency corresponding to the highest power peak in the PSD plot is assigned the center frequency of the mother wavelet. For a given wavelet with scale a, its center frequency is also scaled by the factor F_c/a. If the sampling period of the data, Δ, is also considered, then the frequency corresponding to the wavelet of certain scale, a, is given as:

$$F_a = \frac{F_c}{a.\Delta} \tag{3}$$

Thus, higher scale would represent low frequency and low scale represents the high frequency.

The CWT process can be regarded as the integration over the time duration of the original signal $x(t)$ multiplied by the scaled wavelet. Equation (2) represents the mathematical expression of this process. This process produces wavelet coefficients that are a function of scale and time location. The step-by-step procedure of the CWT process is explained below:

1. Select a mother wavelet.
2. Select the scale range. This step identifies the frequency range of interest because the scale is related to the frequencies.
3. Select the scale interval. This step determines the scale values to be used in the CWT process.
4. Take the wavelet with the initial value of scale and compare it to a section at the start of the original signal $x(t)$ (Figure **3**). Calculate the wavelet coefficient from Equation (2).
5. Shift the scaled wavelet to the new time position and calculate the wavelet coefficients (Figure **4**). This process is continued for the full length of the signal.

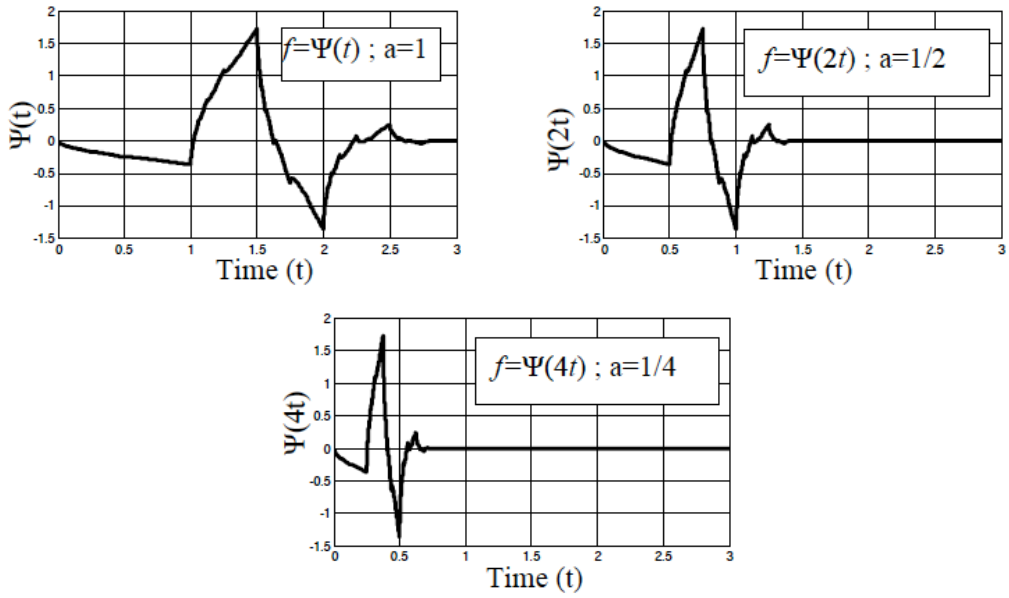

Figure 2: db2 wavelet function with different scales.

6. Scale the mother wavelet according to the scale interval and the scale range and repeat steps 4 and 5.

7. The wavelet coefficient is then plotted either as three dimension or as contour.

The analyzing wavelet that correlates with the properties of the original time varying signal, *x(t)*, provides a greater value of wavelet coefficient, or vice-versa. Since the seismic signal vary rapidly in time domain, its time-frequency plot expected to have a lot of undulation as presented in Figure **5** and Figure **6**. Figure **5** presents the three dimensional plot of wavelet coefficients and Figure **6** presents the contour plot of the same data. Due to undulations in the three dimensional plot, all of the features are difficult to interpret. However, a contour plot provides an effective

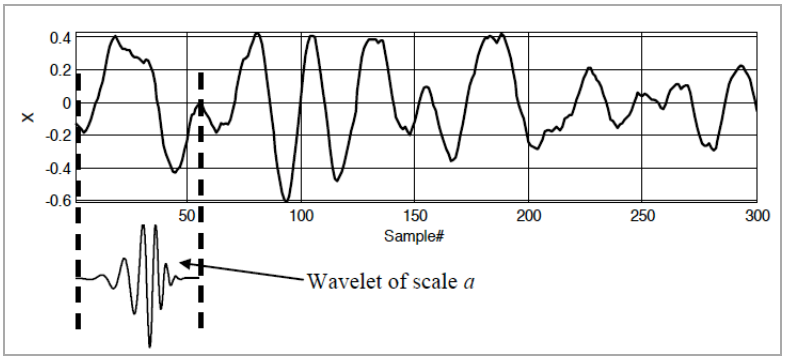

Figure 3: Place the scaled wavelet at the signal origin and calculate wavelet coefficient.

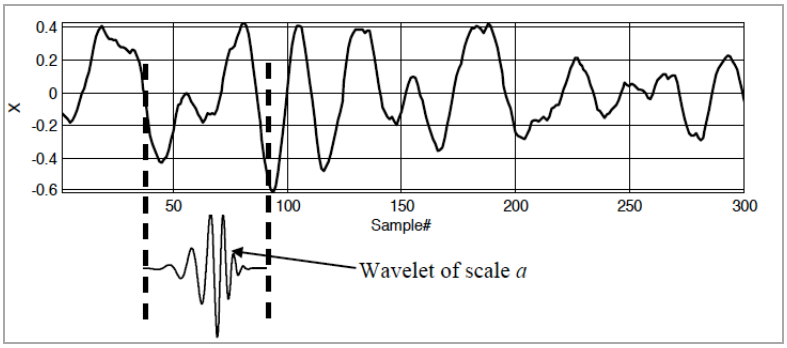

Figure 4: Shift the scaled wavelet to new time location and calculate wavelet coefficient.

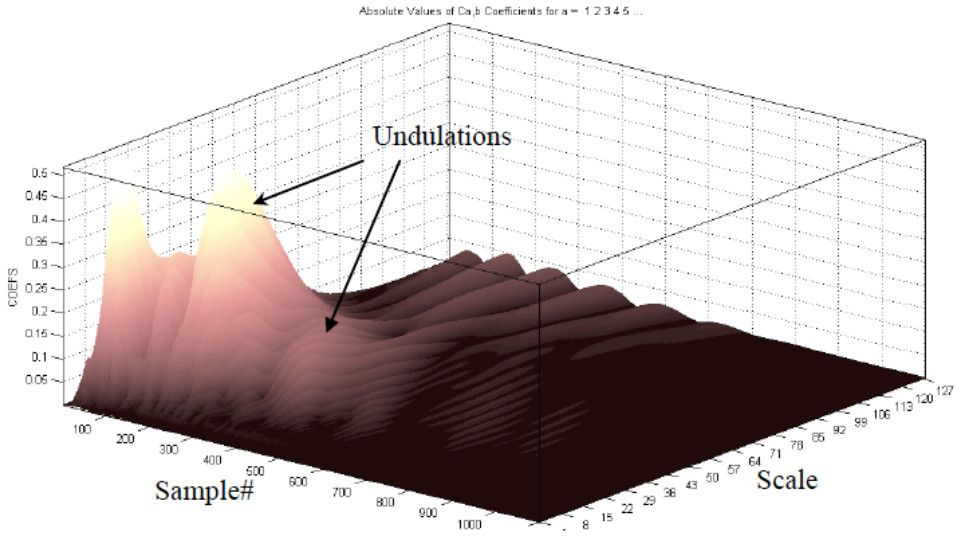

Figure 5: Three dimensional wavelet coefficient plot.

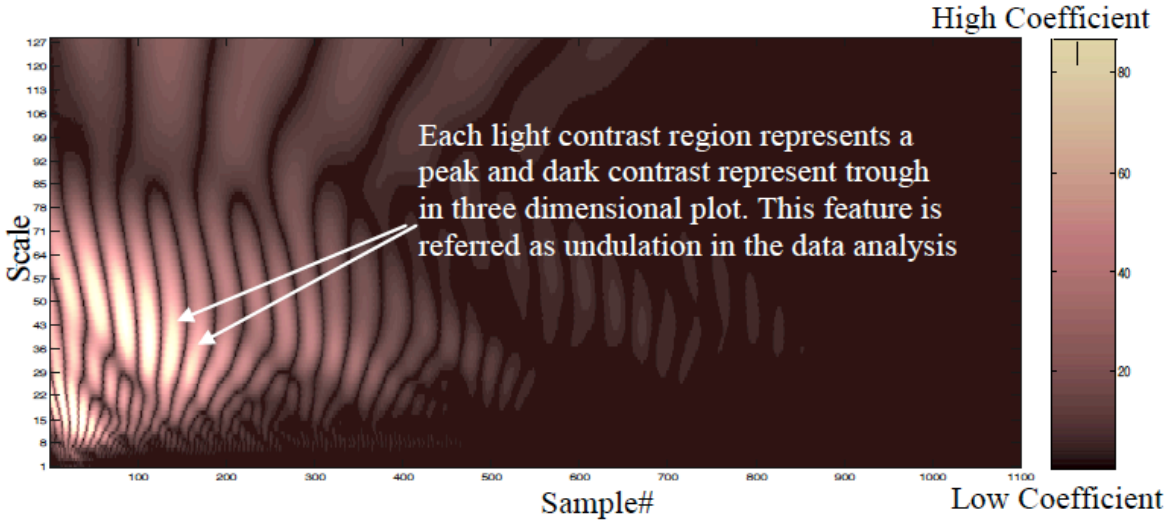

Figure 6: Contour plot of wavelet coefficients.

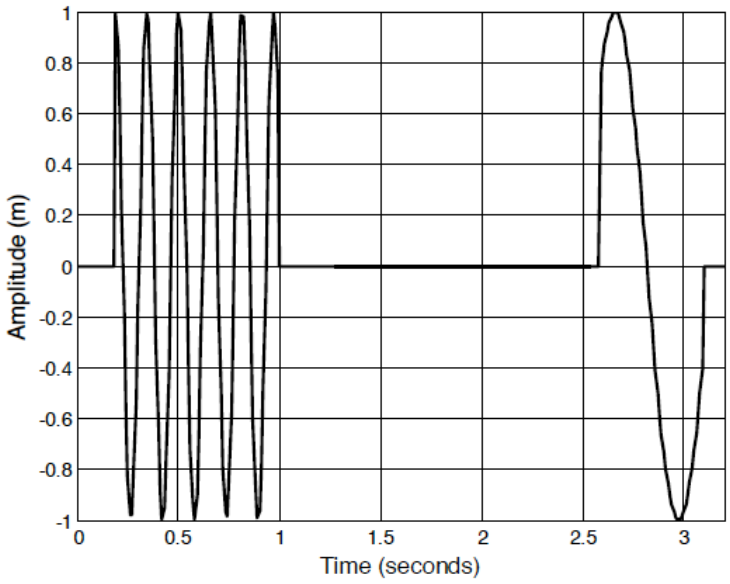

Figure 7: Synthetic signal.

way to study all the features. Thus, in this research, contour plots were used to study the signals rather than three dimensional plots. In Figure **5** the undulations are plotted as ripples in the contour plot. In the analysis, these ripples are referred to as undulations as they are crests and troughs in a three dimensional plot.

Thus, contour plots can be used to extract the information, both in global time and frequency domains, efficiently and accurately. To demonstrate the functionality of wavelet transformations, a synthetic signal of known characteristics presented in Figure **7** and explained by Equation (4) is analyzed and the wavelet coefficient map is generated using the wavelet toolbox of MATLAB® 7.0.

$$\begin{aligned} x(t) &= 00.0 && < t < 0.2 \\ x(t) &= Sin(40t)0.2 && < t < 1.0 \\ x(t) &= 01.0 && < t < 2.6 \\ x(t) &= Sin(10t)2.6 && < t < 3.1 \\ x(t) &= 03.1 && < t < 3.2 \end{aligned} \tag{4}$$

The signal represented by Equation (4) consists of two different frequencies - 40 hertz and 10 hertz respectively. Thus, the PSD of this signal, generated with inbuilt MATLAB® 7.0 functions, consists of two spikes at 10 and 40 hertz (Figure **8**). However, the spectrum plot fails to locate these frequencies in the time domain. CWT was performed with MATLAB® 7.0 on the signal given in Equation (4) and the wavelet

coefficient map was plotted and is presented in Figure **9**.

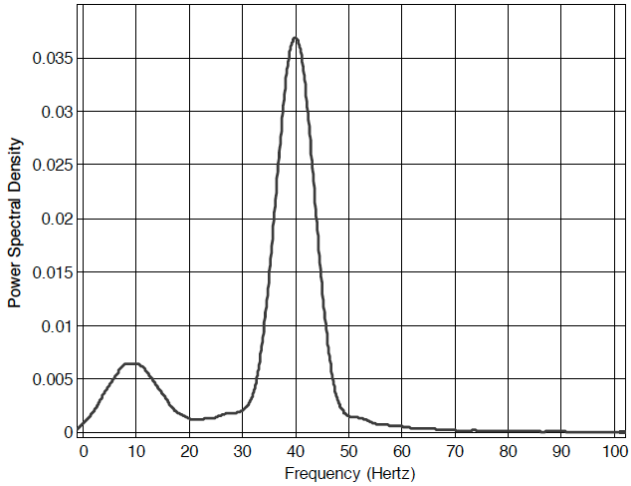

Figure 8: Power spectral density plot of the signal given by equation 3.

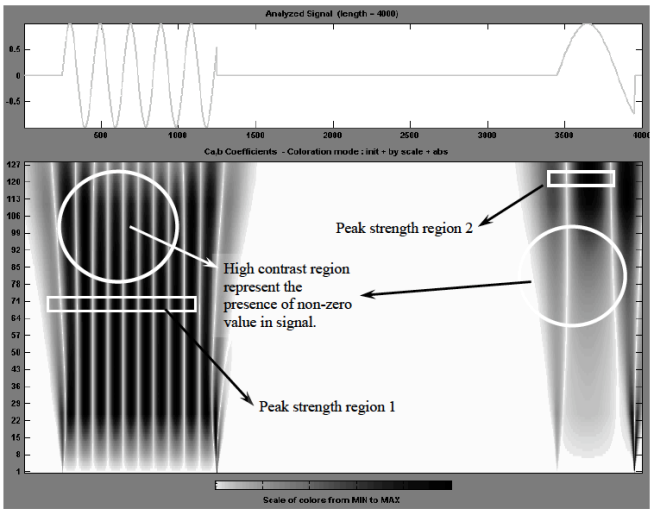

Figure 9: Wavelet coefficient map.

The plot of Figure **9** shows two distinct regions of high color contrast that also correspond to the presence of the non-zero signal in that time range. Also, in the high contrast regions, the maximum color contrast occurs at different scales. In the peak strength region 1, the highest color contrast occurs around scale 71, corresponding to high frequency presence in the corresponding portion of the signal. However, in the peak strength region 2, the highest contrast occurs around scale 120, corresponding to low frequency presence in the corresponding portion of the signal. Thus, it can be concluded from Figure **9** that a wavelet coefficient map is able to provide information about the frequency variation in time and can be used to detect reflected waves from any cavity or obstacle that arrives later than the signal from the incident wave directly from the source.

A single mother wavelet was not used because it would not be capable of analyzing all types of data. The selection of the final mother wavelet relies on the investigator's experience and judgment. The time-frequency plot generated using a particular mother wavelet would be accepted if the characteristic features such as ripples and undulations in the high and low scale regions are distinct. If the features are not distinct, another mother wavelet must be selected. Thus, for a wider range of applicability, families of wavelets are expected to be a more efficient selection.

3. METHODOLOGY

The effect of voids in the soil media was examined by qualitatively comparing the signal properties acquired from controlled laboratory experiments on a soil media, both with and without a void so as to demonstrate proof of concept. For the controlled, experimental study, a wooden box was constructed and filled with readily available, easily managed soil consisting of sand and gravel in two layers. A void of known dimension was excavated in the soil mass in the box at a known location. Seismic waves were produced using a 7.25kg sledge hammer and a rubber mallet. The vertical response of the soil mass surface was recorded using a SignalCalc® 620 Dynamic Signal Analyzer and GiscoTM SN4-4.5Hz digital grade geophones. Finally, data was processed using the MATLAB® 7.0 wavelet toolbox. In addition to the experimental study, a numerical study was conducted. The wave propagation phenomenon was simulated for the laboratory soil box using the finite difference method in the Wave® 2000 Pro software. The experimental and numerical programs are discussed in detail in the following sections.

3.1. Experimental Program

A wooden box of dimension 4.5m × 1.67m × 1.37m ($15' \times 5'6'' \times 4'6''$) was constructed to simulate a limited test sample of layered medium inside a laboratory. The construction of the wooden box is presented in Figure **10**. Initially, the box was filled with two layers: 1) 0.5m ($1'8''$) thick bottom gravel layer; and 2) 0.76m ($2'6''$) thick top sand layer. Both layers were compacted using a powered, mechanical compactor. The in-situ seismic refraction test was performed in the full soil box without a void to determine the soil

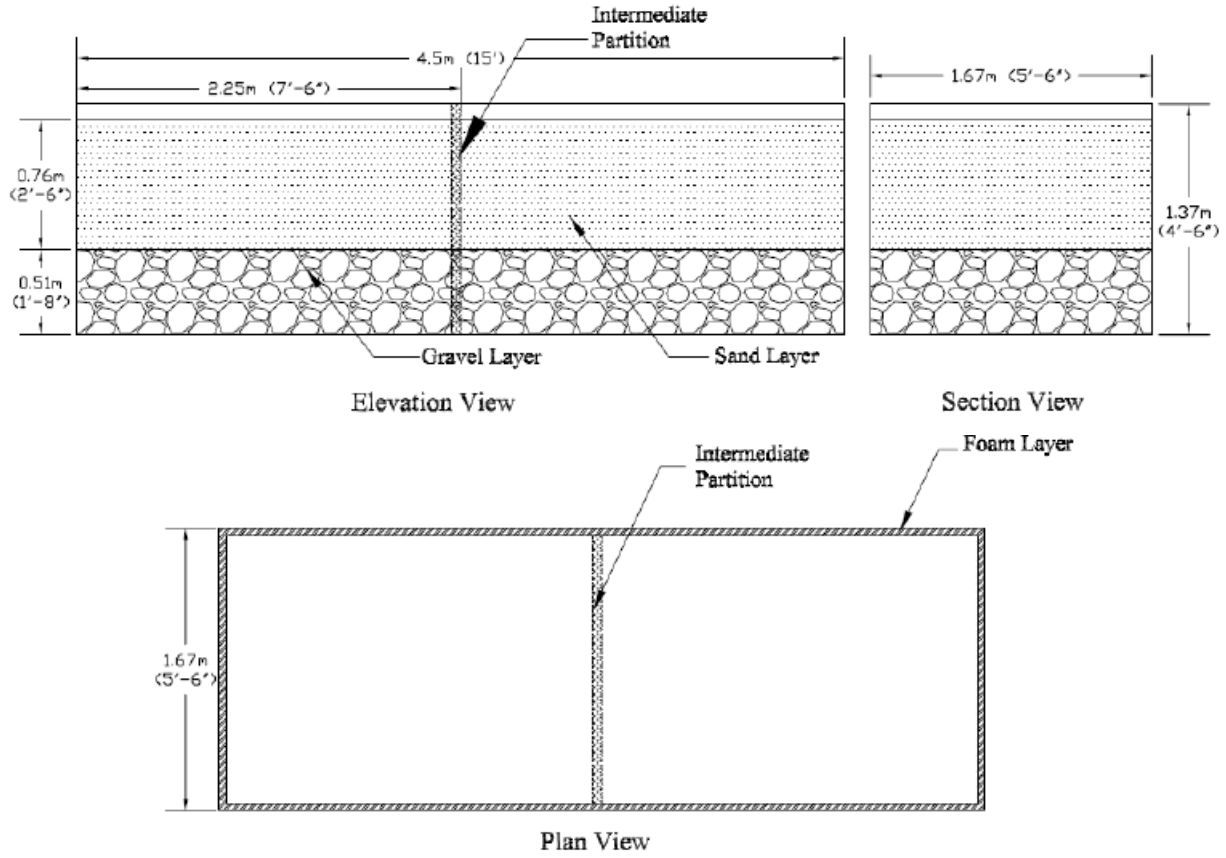

Figure 10: Wooden test box layout.

properties. The void detection test set up consisted of 11 channels with a receiver spacing of 0.305m (1′) from channel 1 to 9. Channel 10 is separated by 0.91m (3′) from channel 9 and 1.22m (4′) from channel 11, as presented in Figure **11**. A void of 0.46m (1′6″) long, 0.91m (3′) wide, and 0.61m (2′) deep was excavated at a distance of 1.14m (3′9″) from the left edge of the soil box. The energy source was placed at channel 1 so that the distance between the energy source and void was maximized and near field effect was minimized. The same soil box test setup was utilized to capture the surface response with no void present.

Channel 1 is at the source location and thus there will be minimal loss of impact energy in the data received. Therefore, this channel was selected for data analysis to approximate impact properties. As the wave travels in the media, it experiences energy loss. There are two main mechanisms for energy loss: damping and dispersion. The damping energy loss is due to the absorption of acoustic energy due to viscosity or other imperfections of the soil media. Dispersion energy loss is due to geometric spreading of the wave front. To study the effects of damping behavior and dispersive behavior, channel 10 was selected because it is located at the maximum distance from the source. Thus, seismic waves experience sufficient energy loss due to both the dispersion effects and damping effects before reaching channel 10. Also, channel 4, located near the center of the soil box, was selected for analysis to observe the change in the dispersion and damping behavior as seismic waves travel across the box. For the soil box test with a void, channel 4 is at a sufficient distance from the void to capture surface wave reflections from the void. The signals from both channels 4 and 10 were analyzed in the time-frequency domain to study the effects of dispersion and damping or reflections from the void in order to mark the signature in time-frequency plots.

3.2. Numerical Simulation of Wave Propagation

The finite difference method is a powerful tool used to solve a large variety of conventional partial differential equations. Due to the simplicity and applicability of this method, finite difference is widely used for solving partial differential equations of wave propagation in the time domain. In this study, Wave2000® Pro Version 2.2 finite difference software was used for numerical simulation. The objective of the

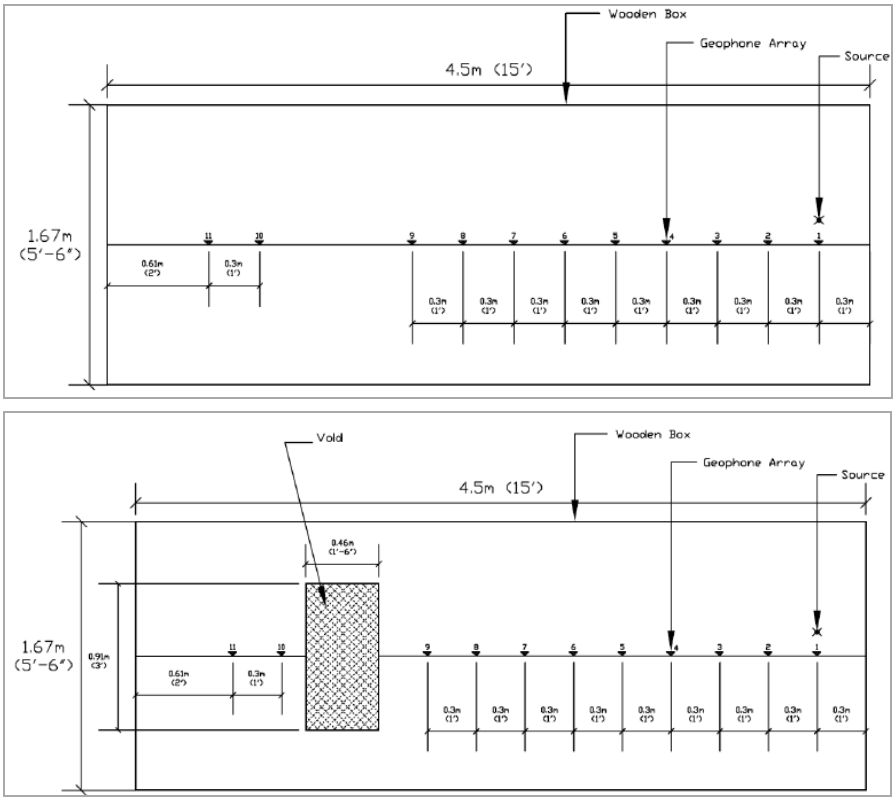

Figure 11(a): Test setup scheme in absence of void. **(b):** Test setup scheme for void detection.

numerical study was to simulate the wave propagation phenomenon in voided elastic media and thus investigate the effect of the voids on the receiver signal time-frequency plot. This also serves to determine if the numerical method accurately simulates such a physical phenomenon.

Dimensions of the numerical simulation problem are 7.2m × 1.5m ($23'7'' \times 4'11''$). Material properties and their distribution taken from the soil box were determined using a refraction test. Figure **12** presents the numerical simulation problem domain and shear wave velocity profile of the elastic media in the simulated soil box. This problem was simulated with three infinite boundary conditions imposed on the left, right, and bottom boundary, and one free boundary condition at the top boundary to simulate the actual ground conditions. The loading pulse was simulated with a function describing a point source, acting on the top surface as discussed by Zerwer, Cascante, and Hutchinson (2002) [11]:

$$\delta(t) = \frac{F_b t}{\pi(t^2 + \psi^2)} \tag{5}$$

In equation (5), F_b alters the magnitude of the excitation, ψ controls the frequency content of the excitation, and t represents time. Source and receiver locations in the numerical simulation model were the same as the geophone locations in the soil box test (Figure **11**(**b**)).

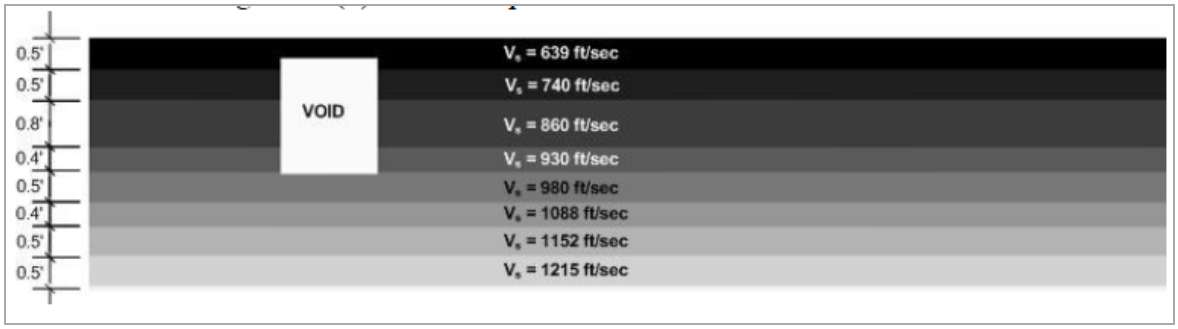

Figure 12: Numerical model setup.

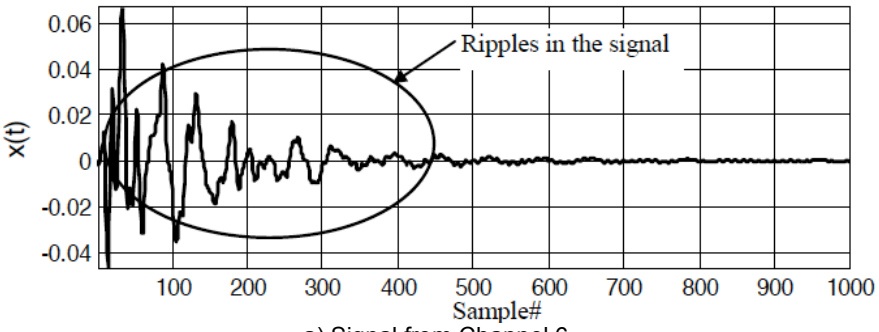

a) Signal from Channel 6

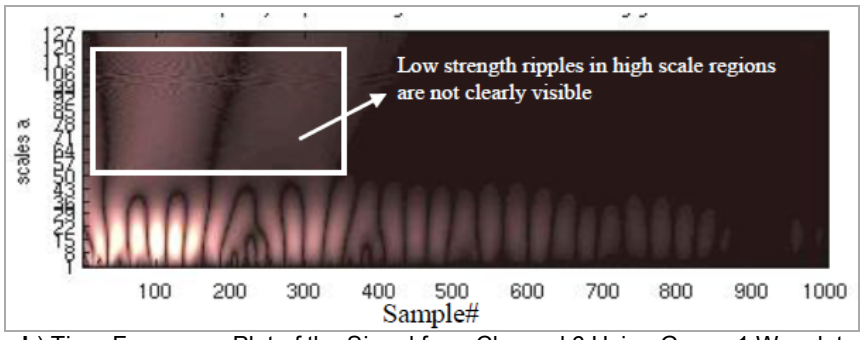

b) Time-Frequency Plot of the Signal from Channel 6 Using Gauss 1 Wavelet

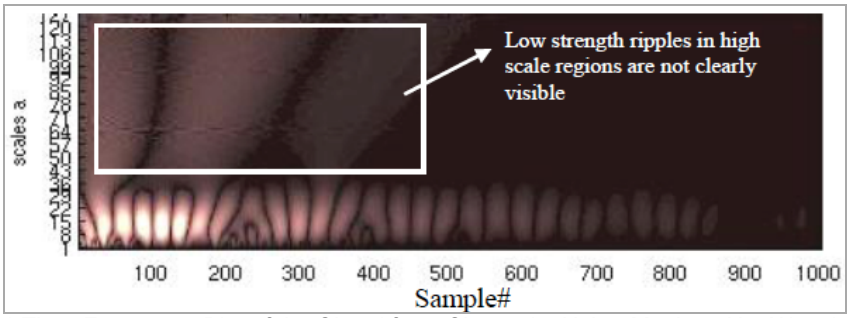

c) Time-Frequency Plot of the Signal from Channel 6 Using Mexican Hat Wavelet

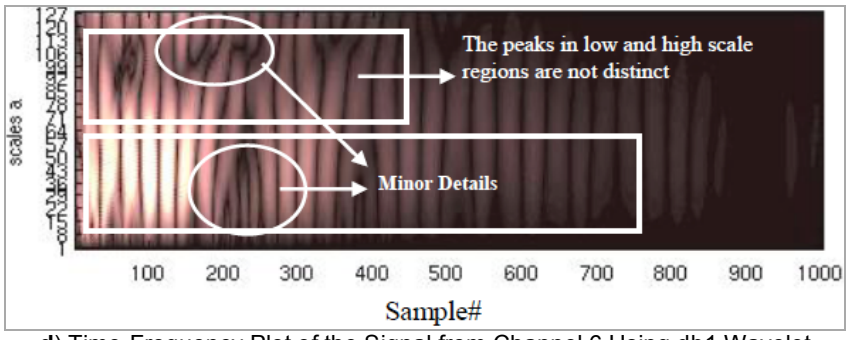

d) Time-Frequency Plot of the Signal from Channel 6 Using db1 Wavelet

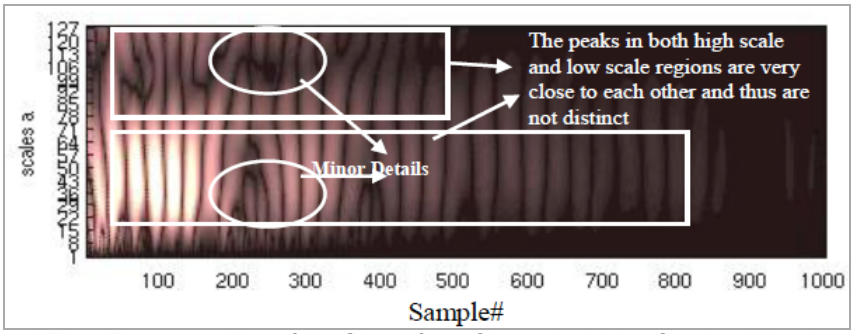

e) Time-Frequency Plot of the Signal from Channel 6 Using Symlet2 Wavelet

Figure 13 continued…

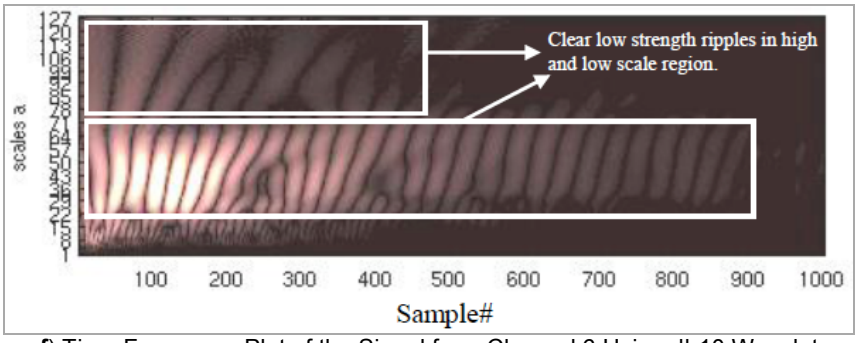

f) Time-Frequency Plot of the Signal from Channel 6 Using db10 Wavelet

Figure 13: Time-frequency plot for channel 6 generated with 7.25kg (**16 lb**) sledgehammer on soil box with void using different types of wavelets.

4. CONTINUOUS WAVELET TRANSFORM ANALYSIS

Laboratory data obtained from soil box tests were analyzed using the MATLAB® 7.0 wavelet toolbox and MATLAB® 7.0 programming platform. Codes were written using the MATLAB® 7.0 programming platform to plot the time-history of the signals from the selected geophones to perform wavelet analyses and to construct time-frequency plots of the geophone data. The data processing was completed in three steps. In the first step, the data from channel 6 was analyzed with different types of wavelets to study the effects of wavelet properties on continuous wavelet transformation. In the second step, channels 1, 4 and 10 of the soil box test setup without a void were analyzed. In the final step, the same selected channels of the soil box test setup with a void were analyzed.

4.1. Analysis Using Different Wavelet Families

The first two time-frequency plots (Figures **13**(**b**) and **13**(**c**)) were generated using the Gaussian and Mexican hat wavelets. The supported width of these wavelets varies from -∞ to +∞ and has a bell shape. However, the signal from the geophone is localized in time, consists of numerous ripples, and is not smooth. Due to differences in the shape of the original signal and the mother wavelet, the CWT eliminates minor details of the signal, and thus high scale (scale 64-128) peaks are not distinct in the time-frequency maps. db1 and symlet2 wavelets have small supported widths and large vanishing points for the supported widths and their shape resembles the original signal. Due to the similarity between the properties of the original signal and these wavelets, the CWT resulted in minor details in the time-frequency maps (Figure **13**), including the noise embedded with the system. These details contaminated the time-frequency map and made the data interpretation task more difficult. A db10 wavelet was used in the final wavelet transformation (Figure **13**(**f**)) because the db10 mother wavelet shape resembles the shape of the original geophone signal and also the properties of the signal. The db10 wavelet resulted in filtering of small ripples caused by noise in the time-frequency plots and thus all the features of the signals in the high scale and low scale regions are distinct (Figure **13**(**f**)). Thus, this wavelet was used in the final data analysis of the signals from the soil box test both with and without a void.

4.2. Wavelet Analysis of Laboratory Soil Box Test Data

A surface wave traveling in an elastic media, with material properties as a function of depth, experiences both dispersion and also material and geometric damping phenomenon. Material and geometrical damping results in signal power loss that is directly proportional to the distance traveled by the surface wave. In the absence of anomalies like voids, surface waves do not encounter obstructions in the wave path, therefore, any observation made in a time-frequency plot of the receiver signal under such conditions can be marked as a signature of the surface wave's damped and dispersive behavior. Seismic tests were conducted on the soil box presented in Figure **11**. The test was performed using a 7.25kg (**16 lb**) sledge hammer and a rubber mallet as an energy source. Time-frequency plots of the selected channels were generated with db10 wavelets for scales from 1 to 128 with a scale interval of 2 and are shown in Figure **14**.

Figures **14**(**a**), **14**(**b**) and **14**(**c**) present time-frequency plots of channels 1, 4, and 10 for data collected during the test conducted without a void and were generated using a 7.25kg (**16 lb**) sledgehammer. Channel 4 and channel 10 signal time-frequency plots

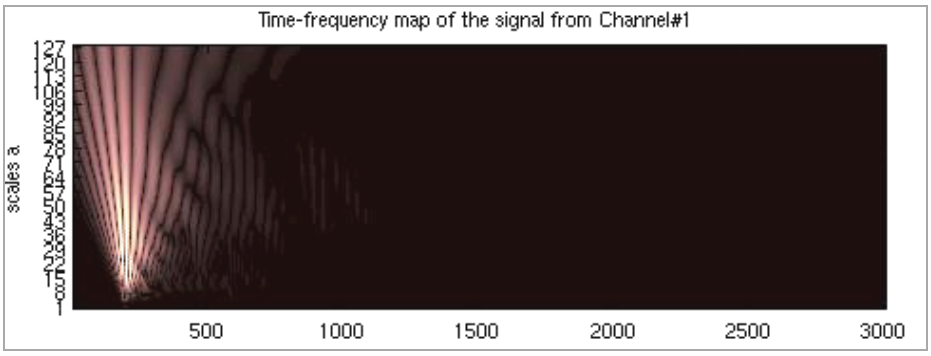

(**a**) Time-frequency Plot of Channel 1

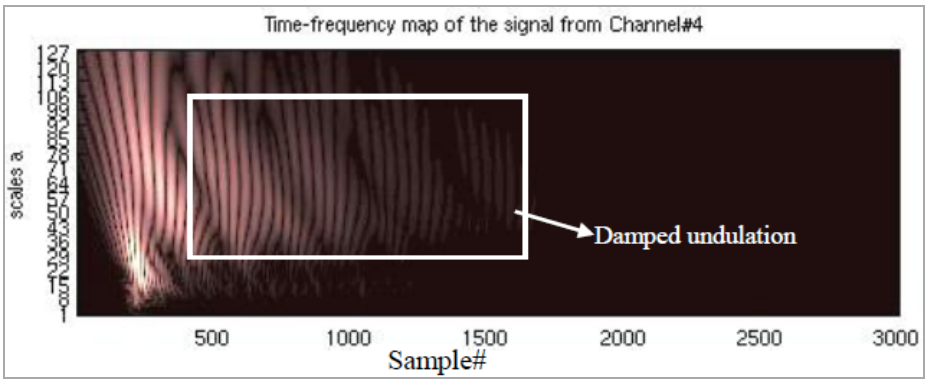

(**b**) Time-frequency Plot of Channel 4

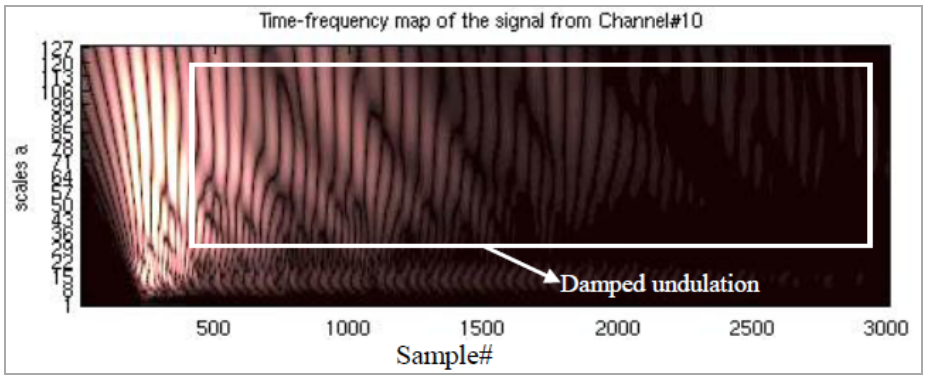

(**c**) Time-frequency Plot of Channel 10

Figure 14: Time-Frequency Plot for Channels 1, 4, and 10 Generated from 7.25kg (**16 lb**) Sledgehammer on Soil Box without Void.

indicate uniformly damped undulations (see Figure **13**(**b**) and **13**(**c**)). However, these undulations are absent in the channel 1 data time-frequency plot (see Figure **13**(**a**)). In the absence of any sub-surface anomalies between channel 1, channel 4 and 10, only dispersion and damping will effect the wave propagation. Thus, it can be concluded that damped uniform undulations in time-frequency plots of the signals from the seismic wave tests is due to dispersion and thus can be marked as the signature of surface wave dispersive behavior. This observation was used in this research to investigate the effect of voids on the signal properties obtained from seismic test on soil box with a void.

For the laboratory test with a void (Figure **11**(**b**)), the same set of channels was analized to permit direct comparisons. Channels 4 and 10 are at a sufficient distance from the source so that waves experience dispersion and damping behaviors. Channel 11 is also at a sufficient distance from the void to capture surface wave reflections from the void. MATLAB® 7.0 was again used to perform continuous wavelet transformation analysis on the data and construct time-frequency plots. Time-frequency plots were generated with db10 wavelets for scales from 1 to 128 with a scale interval of 2.

Figures **15**(**a, b** and **c**) present channels 1, 4, and 10 data time-frequency plots generated as a result of a 7.25kg (**16 lb**) sledgehammer impact on the soil medium with a void. The channel 4 signal time-frequency plot shows the signature of dispersion behavior as damped uniform undulations (see Figure **15**(**b**)), the same as concluded from the seismic test in the soil box without a void. Unique low strength ripples in the high scale (low frequency) region between samples 300 and 700 can also be observed in this time-frequency plot. However, these low strength ripples are not present in the channel 4 signal time-frequency plot obtained from the soil box test without the void (Figure **14**(**b**)). Therefore, it can be concluded that low strength and high scale ripples are occurring due to the reflections from the void surface because it is the only difference in the test setups and thus can be identified as the signature of the void-like anomaly. The channel 10 signal time-frequency plot (Figure **15**(**c**)) also shows the same damped uniform undulations as observed in the channel 10 signal time-frequency plot (Figure **14**(**c**)) obtained from the soil test without the void. However, low strength, low frequency ripples as observed in the channel 4 signal time-frequency plot (Figure **15**(**b**)) are absent. From this observation it can be concluded that the void or anomalies do not disrupt

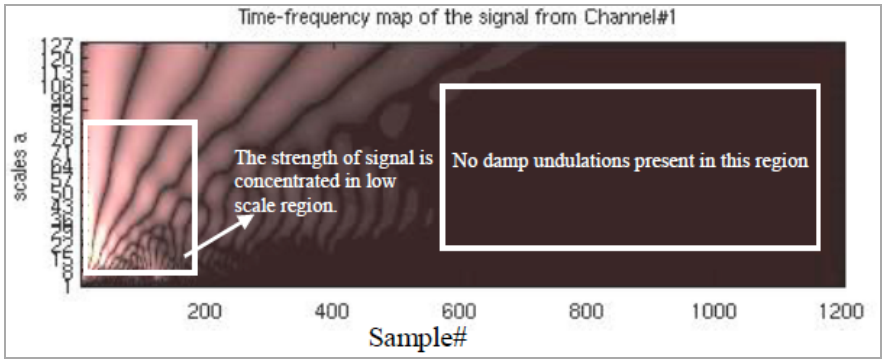

(**a**) Time-frequency Plot of Channel 1

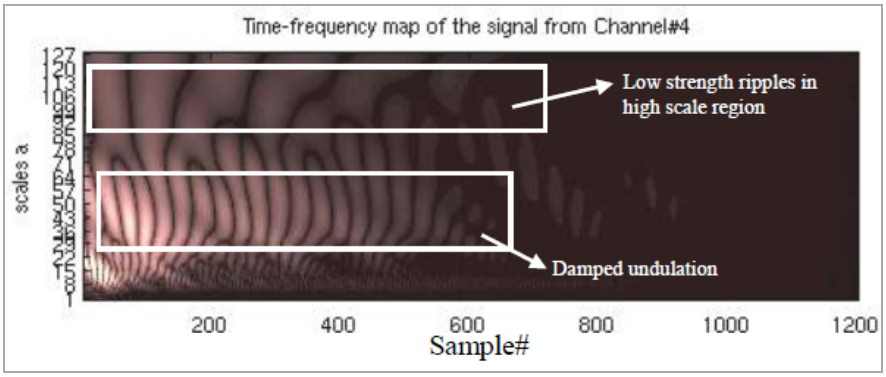

(**b**) Time-frequency Plot of Channel 4

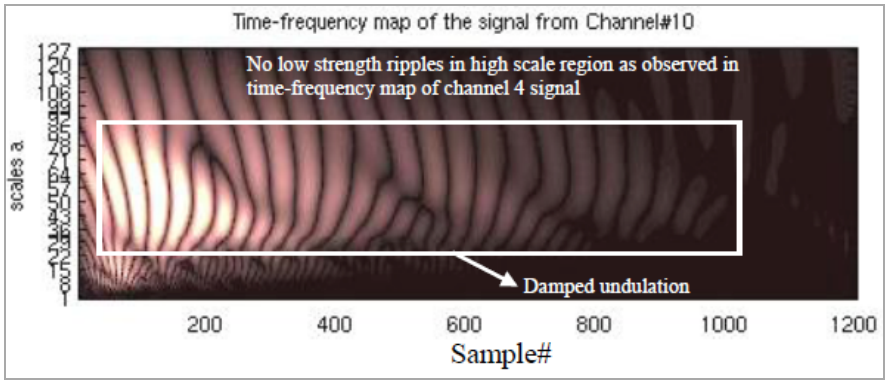

(**c**) Time-frequency Plot of Channel 10

Figure 15: Time-frequency plot for channels 1, 4, and 10 generated from rubber mallet on soil box with void.

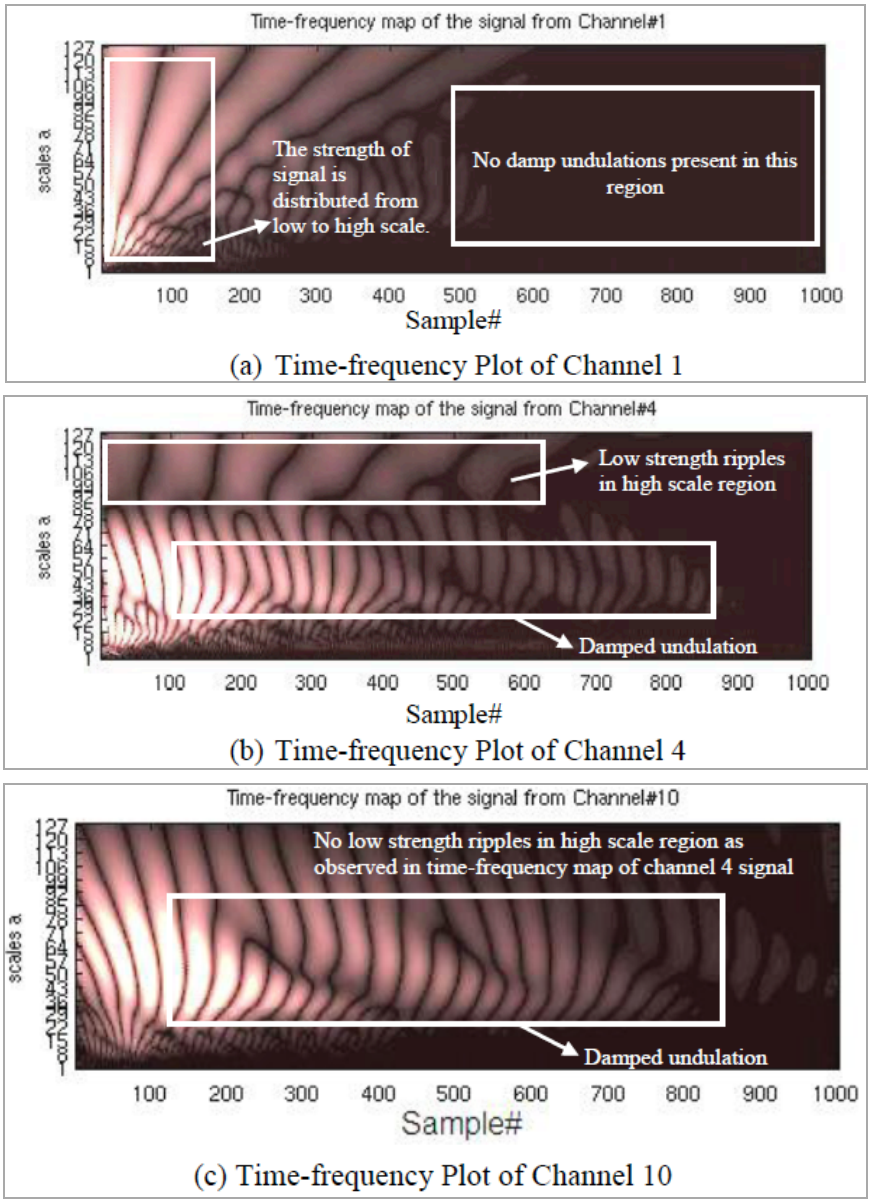

Figure 16: Time-frequency plot for channels 1, 4, and 10 generated from 7.25kg (**16 lb**) sledgehammer on soil box with void.

the time-frequency spectrum of the signals from geophones placed after the void or anomalies.

A final set of laboratory tests were conducted on the soil box test setup with a void. A rubber mallet was used as the energy source. MATLAB® 7.0 was used to perform continuous wavelet transformation analysis on the data and construct time-frequency plots. Time-frequency plots were generated with db10 wavelets for scales from 1 to 128 with a scale interval of 2. Time-frequency plots for channels 1, 4, and 10 data are presented in Figure **16**.

Figures **15**(**a**) and **16**(**a**) present the time-frequency plots of the data from channel 1, located at the source, and generated as a result of an impact from a 7.25kg (**16 lb**) sledgehammer and a rubber mallet respectively. For a 7.25kg (**16 lb**) sledgehammer impact, the major portion of energy lies between 2 to 85, however, for a rubber mallet impact, the major portion of energy lies between scales 2 to 57. Thus, an impact from a rubber mallet produces waves with a major portion of energy in the high frequency (low scale) region, however, high frequency waves have a higher attenuation rate than low frequency waves (Zerwer, 2002). Thus, the channel 4 CWT response as a result of a rubber mallet impact demonstrates that the dispersion phenomenon decays at a higher rate than the signal from a sledgehammer impact. (Figure **15**(**b**) and Figure **16**(**b**)). However, CWT plot characteristics are the same, not only for channel 4 but also for channel 10, which is

characterized by the absence of low strength and high scale ripples. Thus, time-frequency plots of channels 1, 4 and 10 data generated as a result of a rubber mallet impact on the void test setup (Figure **16**(**a**), **16**(**b**) and **16**(**c**)) confirm the conclusions from the data analysis of the signals as a result of a sledgehammer impact. From this data analysis, it can also be concluded that the dispersion effects or damping effects signature and void signature in the time-frequency domain do not change with source weight.

4.3. Wavelet Analysis of the Numerical Simulation Data

Seismic tests conducted on the soil box were simulated using Wave 2000® Pro Version 2.2 and the receiver data was processed using the same protocol that was used for the laboratory test data. Time-frequency plots were generated with db10 wavelets for scales from 1 to 128 with a scale interval of 2. Plots for receivers 1, 4, and 10 are presented in Figure **17**.

The channel 4 data time-frequency plot (Figure **17**(**b**) presents uniform undulations, both in high scale as well as low scale regions. Geometric damping causes the surface wave dispersion to decay in the low scale region, but the decay rate is less than the decaying observed in the experimental results because material damping was not considered in the numerical simulation model. Attenuation is a very complex phenomenon for simulation of wave propagation in a dispersive media and it is also difficult to measure

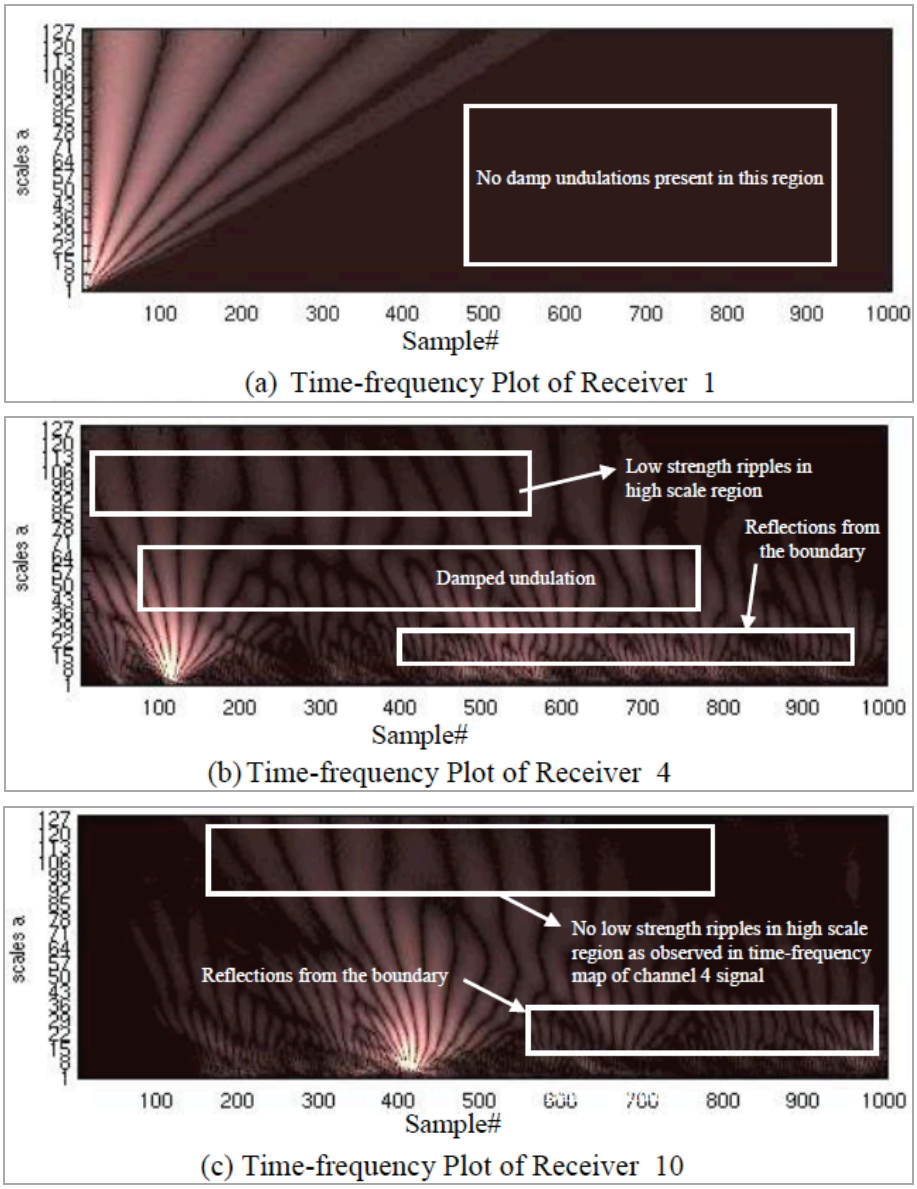

Figure 17: Time-frequency plot of receivers 1, 4, and 10 generated from numerical simulation.

experimentally, thus it was not considered in the study scope. The time-frequency plot of channel 4 data presents a unique time-frequency spectrum signature of voids as low strength ripples in the time-frequency domain in the high scale (low frequency) region between sample 350 and 700, similar to the laboratory test results, that are absent from both the channel 1 and channel 10 data time-frequency plots. This channel 4 plot also shows the some reflections from the infinite boundaries that are contaminating the plot. Because the material attenuation was not considered in this numerical simulation, these reflections were not absorbed by the material. These reflections were not present in the experimental data time-frequency plot because the material had its inherent damping that permitted absorption of any reflection from the boundary. The channel 10 data time-frequency plot consists of the dispersion behavior time-frequency signature but no low-strength, high-scale signature of voids, which confirms the conclusions from the laboratory data analysis. This time-frequency plot has same reflections as the channel 4 time-frequency plot has infinite boundary and could not eliminate them.

5. SUMMARY AND CONCLUSIONS

This research investigated the effect of anomalies such as voids on surface wave propagation by studying the signal in the time-frequency domain using CWT. The study also investigated the effects of different types of wavelets on the CWT and developed a protocol for the processing of seismic wave data for void detection. Research was conducted in several steps: the first step in the research program was to develop a controlled experiment to study surface wave propagation in voided soil media. A wooden box was constructed and filled with sand and gravel in two layers. A void of known dimension was excavated in the soil mass at a known location. A refraction test was conducted on the soil mass in the wooden mass to compute the in-situ shear wave velocity profile of the soil mass with the objective of creating a material model and its spatial distribution for the finite difference simulation capable of replicating the results from the micro-seismic testing. A numerical simulation model was created only for the surface wave propagation in voided soil mass.

Based on the present research, it can be concluded that different wavelet families can be used in CWT analysis to study the seismic data signal properties localized in the time domain. During the CWT analysis, the shape and the properties of the mother wavelet influence the analysis. The time-frequency plot features generated from a CWT analysis can be used to investigate the seismic wave propagation and thus can be used to study its properties.

The time-frequency plot of the signal generated using sledgehammer on the soil box test without a void shows damped uniform undulations from low to high scales. In the absence of any sub-surface anomalies in the soil box, only dispersion and damping will effect the wave propagation. Thus, damped uniform undulations in time-frequency plot of the signals from the seismic wave tests can be marked as the signature of surface wave dispersive behavior.

The time-frequency plot of the signal generated using a sledgehammer on the soil box test with a void shows low-strength ripples in time-frequency plots, usually in the high scale (low frequency) region apart from the damped uniform undulations from low to high scales. These low-strength ripples in the high-scale region of the time-frequency plot of the signals from the seismic wave tests can be marked as the signature of the void-like anomaly. The low-strength high-scale ripples were only observed in the time-frequency plot of the data from the channels between the void and the source. However, these ripples are absent from the time-frequency plot of the signal from the channel placed after the void. Thus, the void or anomalies do not disrupt the time-frequency spectrum of the signals from geophones placed after the void or anomalies.

The time-frequency plot of the signal generated using a rubber mallet on the soil box confirms the conclusions from the signal analysis of a sledgehammer impact. Thus, the dispersion or damping behavior signature and void signature in time-frequency domain do not change with source weight.

For a sledgehammer impact, the major portion of energy lies between 2 to 85, however, for a rubber mallet impact, the major portion of energy lies between scales 2 to 57. Thus, impact from the lighter weight energy source produces waves with a major portion of energy in the high frequency (low-scale) regions and heavier energy source produces waves of both high and low frequencies.

The present study focused on the effect of void-like anomalies on surface wave propagation by studying the signal in the time-frequency domain using continuous wavelet transformation. A parametric study to fully understand the effects of size and shape of

voids on the time-frequency domain would be valuable. In addition, it would be useful to perform field experiments and analyze the seismic data using the wavelet transformation.

REFERENCES

[1] Dobecki TL and Upchurch SB. Geophysical Applications to Detect Sinkholes and Ground Subsidence. The Leading Edge 2006; 25; 3; 336-341. http://dx.doi.org/10.1190/1.2184102

[2] Cooper SS and Ballard RF. Geophysical Exploration for Cavity Detection in Karst Terrain. Proceeding of Symposium on Geotechnical Aspects Karst Terrain: Exploration, Foundation Design and Performance and Remedial Measures; Geotechnical Special Publication No. 14; ASCE; New York 1988; pp 25-39.

[3] Belesky RM and Hardy HR. Seismic and Microseismic Methods for Cavity Detection and Stability Monitoring of Near Surface Voids. Proceeding of 27th US Symposium on Rock Mechanics: Key to Energy Production, University of Alabama, Tuscaloosa, Alabama 1986; 1: 248-258.

[4] Dravinski M. Ground Motion Amplification Due to Elastic Inclusions in a Half-space. Earthquake Engineering and Structure Dynamics 1983; 11(3): 313-335. http://dx.doi.org/10.1002/eqe.4290110303

[5] Curro JR. Cavity Detection and Delineation Research. Report 2, Seismic Methodology 1983; Medford Cave Site; Florida, U.S. Army Waterway Experiment Station Technical Report GL-83-1; U.S. Army Waterway Experiment Station; Vicksburg; Mississippi.

[6] Ganji V, Gucunski N and Maher M. Detection of Underground Obstacles by SASW Method: Numerical Aspects. Journal of Geotechnical and Geoenvironmental Engineering 1997; 123(3): 212-219. http://dx.doi.org/10.1061/(ASCE)1090-0241(1997)123:3(212)

[7] Shrivastava A. Detection of Subsurface Voids in Stratified Media Using Seismic Wave Methods. Master of Science Thesis. Department of Civil and Environmental Engineering, The Pennsylvania State University 2009.

[8] Kaiser G. A friendly Guide to Wavelets. Boston: Birkhauser Publishing 1994.

[9] Walker JS. A Primer on Wavelets and Their Scientific Applications. Florida: CRC Press 1999. http://dx.doi.org/10.1201/9781420050011

[10] Walnut D. Introduction to Wavelet Analysis. Boston: Birkhauser Publishing 2002.

[11] Zerwer A, Cascante G and Hutchinson J. Parameter Estimation in Finite Element Simulations of Rayleigh Waves. Journal of Geotechnical and Geoenviromental Engineering 2002; 128(3): 250-261. http://dx.doi.org/10.1061/(ASCE)1090-0241(2002)128:3(250)

Received on 22-12-2015 Accepted on 20-03-2016 Published on 31-07-2016

DOI: http://dx.doi.org/10.15377/2409-5710.2016.03.01.1